

1 **Intermittent hypoxia mediated by TSP1 dependent on STAT3 induces cardiac fibroblast**
2 **activation and cardiac fibrosis**

3 Qiankun Bao¹, Bangying Zhang¹, Ya Suo¹, Chen Liu², Qian Yang¹, Kai Zhang¹, Ming Yuan¹,
4 Meng Yuan¹, Yue Zhang¹, Guangping Li¹

5 ¹Tianjin key laboratory of Ionic-Molecular Function of Cardiovascular Disease, Department
6 of Cardiology, Tianjin Institute of Cardiology, the Second Hospital of Tianjin Medical
7 University, Tianjin, China;

8 ²Department of Clinical Laboratory, Peking University People's Hospital, Beijing, China.

9 **Running title** : Role of TSP1 in intermittent hypoxia induced-cardiac fibrosis

10 Correspondence should be addressed to Qiankun Bao (baoqiankun@tmu.edu.cn), or
11 Guangping Li (tic_tjcardiol@126.com)

12 Qiankun Bao, MD, PhD,

13 Tianjin key laboratory of Ionic-Molecular function of cardiovascular disease, Department of
14 Cardiology, Tianjin institute of cardiology, the second hospital of Tianjin Medical University,
15 300211, Tianjin, China,

16 Tel: 86-22-88326237,

17 E-mail: baoqiankun@tmu.edu.cn

18 **Abstract**

19 Intermittent hypoxia (IH) is the predominant pathophysiological disturbance in obstructive
20 sleep apnea (OSA), known to be independently associated with cardiovascular diseases.
21 However, the effect of IH on cardiac fibrosis and molecular events involved in this process
22 are unclear. Here, we tested IH in angiotensin II (Ang II)-induced cardiac fibrosis and
23 signaling linked to fibroblast activation. IH triggered cardiac fibrosis and aggravated Ang
24 II-induced cardiac dysfunction in mice. Plasma thrombospondin-1 (TSP1) content was
25 upregulated in both IH-exposed mice and OSA patients. Moreover, both *in vivo* and *in vitro*
26 results showed IH-induced cardiac fibroblast activation and increased TSP1 expression in
27 cardiac fibroblasts. Mechanistically, phosphorylation of STAT3 at Tyr705 mediated the
28 IH-induced TSP1 expression and fibroblast activation. Finally, STAT3 inhibitor S3I-201 or
29 AAV9 carrying a periostin promoter driving the expression of shRNA targeting Stat3
30 significantly attenuated the synergistic effects of IH and Ang II on cardiac fibrosis in mice.
31 This work suggests a potential therapeutic strategy for OSA-related fibrotic heart disease.

32 **Keywords:** intermittent hypoxia, cardiac fibrosis, cardiac fibroblast activation, STAT3, TSP1

33 **Introduction**

34 The prevalence of sleep apnea is high in patients with cardiovascular disease, which could be
35 caused by multiple risk factors including respiratory instability, obesity and upper airway
36 dysfunction^{1, 2}. Sleep apnea, classified as obstructive sleep apnea (OSA) and central sleep
37 apnea, affects or covaries with numerous health outcomes and physiological processes,
38 particularly cardiovascular disease¹⁻³. A recent prospective study of OSA found it associated
39 with increased risk of incident heart failure in community-dwelling middle-aged and older
40 men⁴. OSA is associated with a profile of perturbations that include sympathetic nerve activity,
41 metabolic dysregulation, inflammation, oxidative stress, vascular endothelial dysfunction, and
42 intermittent hypoxia (IH), all of which are critical for the pathogenesis of coronary heart
43 disease, hypertension, atrial fibrillation, and heart failure^{1, 2}. IH is a hallmark of OSA and
44 initiates several mechanisms that lead to cardiac fibrosis and cardiac dysfunction^{5, 6}.

45 Cardiac fibrosis is characterized by excessive deposition of extracellular matrix proteins by
46 cardiac fibroblasts (CFs), which respond to pathological stress and environmental stimuli by
47 transforming into myofibroblasts. Activated CFs express elevated levels of various
48 proinflammatory and profibrotic factors causing fibroblast proliferation, migration and scar
49 formation⁷. The persistence of myofibroblasts eventually results in adverse changes in
50 ventricular structure and compliance, thereby leading to heart failure^{5, 7}. However, the effect
51 and mechanism of CF activation in IH-induced cardiac remodeling remain unclear.

52 One central cytokine linked to cardiac fibrosis is transforming growth factor β (TGF β), which
53 is highly regulated at the level of activation^{7, 8}. The activation of latent pro-TGF β requires
54 thrombospondin-1 (TSP1, encoded by *Thbs1* gene), which is a matricellular glycoprotein and
55 can be secreted by various cell types, to remove its latency-associated propeptide⁸⁻¹⁰.
56 Myocardial TSP1 expression was increased in a mouse model of pressure overload because of
57 transverse aortic constriction¹¹, and blocking TSP1-dependent TGF β activation prevented
58 cardiac fibrosis progression and improved cardiac function¹². However, the role and

59 underlying mechanism of TSP1 in IH-induced CF activation and cardiac fibrosis remain to be
60 elucidated.

61 As a member of the signal transducer and activator of transcription (STAT) protein family,
62 STAT3 was originally identified as an interleukin-6-activated transcription factor. It can also
63 be phosphorylated by receptor-associated Janus kinase (JAK) in response to growth factor and
64 hemodynamic stress, thus acting as a regulator in fundamental cellular processes including
65 inflammation, cell growth, proliferation, differentiation, migration, and apoptosis¹³⁻¹⁵.
66 Emerging evidence demonstrates that STAT3 signaling is hyperactivated in fibrotic diseases,
67 which may be an important molecular checkpoint for tissue fibrosis^{14, 16}. Recent study
68 demonstrated that STAT3 can drive TSP1 expression in astrocytes¹⁷. Given the integrated
69 function of STAT3 activation in inflammation and fibrosis, we hypothesized that IH-induced
70 STAT3 activation might play a crucial role in CF activation and cardiac fibrosis by increasing
71 TSP1 expression.

72 In the present study, we investigated the effect of IH exposure on cardiac fibrosis in response
73 to angiotensin II (Ang II) in mice and the potential underlying mechanism. TSP1 expression
74 induced by IH in CFs, mediated by phosphorylation of STAT3 at Tyr705, was involved in CF
75 activation and cardiac fibrosis. Pharmacological or genetic inhibition of STAT3 restrained
76 IH-induced CF activation and cardiac fibrosis and ameliorated IH-induced cardiac
77 dysfunction.

Results

IH induced cardiac fibrosis and aggravated Ang II-induced cardiac dysfunction in mice.

Most respiratory events of patients with OSA result in desaturation–reoxygenation sequences that cause IH⁵. To investigate IH exposure to cardiac function, we housed mice under IH or normoxia for 28 days (Figure 1A). Hypoxia in heart tissue was evaluated by using pimonidazole (Figure 1-figure supplement 1A). IH exposure slightly increased the ratio of heart weight to tibial length (Figure 1B). Echocardiography analysis revealed a moderate decrease in ejection fraction (EF) and fractional shortening (FS) with IH as compared with normoxia (Figure 1C-D). Furthermore, Masson and Sirius red staining demonstrated mildly larger fibrosis area in the heart of mice after IH exposure (Figure 1E-F).

To investigate the effect of IH associated with cardiac function after injury, we used the mouse model of Ang II-induced cardiac hypertrophy to represent cardiac fibrotic responses. Consistent with previous studies^{16, 18}, Ang II treatment induced cardiac fibrosis with increasing the ratio of heart weight to tibial length and fibrosis area and impaired EF and FS (Figure 1B-D). Strikingly, IH exposure further impaired cardiac function, with increasing the ratio of heart weight to tibial length and decreasing EF and FS (Figure 1B-D). IH exposure significantly enlarged the fibrotic area of heart as well (Figure 1E-F). IH exposure had little effect on myocyte size or ratio of apoptotic cells in the left ventricle with or without Ang II challenge (Figure 1-figure supplement 1B-C). These results indicated that IH could induce cardiac fibrosis both at the basal level and in response to Ang II and also aggravated Ang II-induced cardiac dysfunction.

IH induced fibroblast activation in myocardial interstitium.

CFs are now recognized for their fundamental contributions to the heart's response to various forms of injury⁷. To investigate the effect of IH on fibroblast activation, we analyzed the

expression of α -SMA, collagen I and periostin in the left ventricle of mice after IH exposure. First, immunofluorescence staining showed strongly α -SMA signaling in vimentin-positive CFs in the IH group. IH-induced α -SMA expression in CFs was further enhanced under the Ang II-induced cardiac pathologic condition (Figure 1G-H). Meanwhile, the expression of collagen I and periostin showed a similar trend as α -SMA expression (Figure 1G-H). In addition, IH exposure slightly increased the mRNA and protein levels of α -SMA, collagen I and periostin (Figure 1I-K) in the mouse left ventricle and significantly elevated the levels in the left ventricle of Ang II-infused mice (Figure 1I-K). These results suggest that IH can activate CFs at the basal level and under the Ang II-induced injury condition.

IH exposure promoted TSP1 expression in CFs.

To test whether TSP1 plays an important role in the progression of cardiac fibrosis induced by IH, we next detected TSP1 expression in mice after IH exposure. As compared with normoxia, IH exposure significantly increased plasma TSP1 content and mRNA level in the mouse left ventricle, especially in Ang II-infused mice (Figure 2A-B). The protein level of TSP1 in the left ventricle showed a similar trend to that of collagen I and periostin (Figure 2C-D). Given that TGF β and its downstream Smad signaling critically modulate the fibroblast phenotype^{7, 19}, we assessed Smad2/3 phosphorylation in the mouse left ventricle. The phosphorylation of Smad2/3 was slightly increased after IH exposure but greatly increased after IH exposure in the Ang II-induced injury condition (Figure 2C-D), which is consistent with TSP1 expression. Furthermore, immunofluorescence staining showed elevated signaling of TSP1 in the left ventricle after IH, especially in the Ang II-induced condition (Figure 2E-F). In addition, the expression of TSP1 in cells positive for Thy1 (an inclusive surface protein given its association with CFs^{20, 21}) and negative for CD11b (macrophage marker), CD31 (endothelial cell marker), CD45 and Ter119 (hematopoietic cell marker) in the heart, detected by flow cytometry, was significantly higher after IH exposure (Figure 2G), which indicated that IH exposure could induce TSP1 expression in CFs.

To identify the potential relevance of TSP1 to OSA, we measured the concentration of TSP1 in plasma samples from 21 patients with OSA and 21 healthy subjects. TSP1 content was significantly increased in patients with OSA as compared with healthy individuals (Figure 2H). Together, these data suggest that TSP1 level was elevated in both mice and humans after IH exposure and might contribute to CF activation and cardiac fibrosis.

IH induced primary CF (PCF) activation via TSP1.

Next, to confirm the effect of IH on PCF activation *in vitro*, we used immunofluorescence staining of α -SMA in mouse PCFs (mPCFs) with or without IH exposure. As compared with normoxia, IH increased α -SMA expression in PCFs and led to an activated phenotype of fibroblast cells (Figure 3A-B). In addition, IH exposure increased the proliferation and contractility of PCFs (Figure 3C-D). We tested whether TSP1 plays an important role in fibroblast activation and found the mRNA expression of *Thbs1* significantly increased by IH as compared with normoxia in mPCFs (Figure 3E). In addition, IH significantly increased the protein level of TSP1 beginning from 2 hr and sustained until 8 hr in mPCFs (Figure 3F-G). Furthermore, shRNA lentivirus used to produce TSP1 deficiency in PCFs attenuated IH-induced mRNA and protein levels of α -SMA, collagen I and periostin (Figure 3H-K). TSP1 deficiency in PCFs also blocked inflammatory gene *Tnfa* expression (Figure 3I) induced by IH exposure. Thus, our results suggested that IH induced PCF activation through upregulating TSP1.

IH upregulated phosphorylation of STAT3 at Tyr705 site both *in vivo* and *in vitro*.

TSP1 was reported to be transcriptionally regulated by STAT3 in astrocytes¹⁷, and emerging evidences has indicated that STAT3 involved in fibrosis diseases^{14, 22}. Here, we hypothesized that STAT3 might play a vital role in IH-induced TSP1 expression and cardiac fibrosis. Since the phosphorylation status of STAT3 is related to its transcriptional activity^{23, 24}, we determined the phosphorylation of STAT3 at multiple sites as well as the phosphorylation of

JAKs in mPCFs under IH. STAT3 phosphorylation at Tyr705 was significantly increased by IH from 0.5 to 2 hr, but STAT3 phosphorylation at Ser727 or total STAT3 was not altered by IH exposure (Figure 4A-B). Meanwhile, IH exposure significantly induced the phosphorylation of JAK2 at Tyr1008 without affecting that of JAK1 or JAK3 (Figure 4A-B). A JAK2 inhibitor, TG101209, abolished the phosphorylation of STAT3 at Tyr705 induced by IH (Figure 4C-D), so IH-induced STAT3 phosphorylation might be mediated by JAK2. Phosphorylation of STAT3 at Tyr705 was reported to be crucial to STAT3 nuclear translocation and transcriptional activity^{23, 24}, so we next analyzed the STAT3 subcellular localization. STAT3 nuclear translocation was significantly increased by IH on immunofluorescent staining (Figure 4E-F). Moreover, in the mouse left ventricle after IH exposure, consistent with results *in vitro*, IH exposure induced phosphorylation of STAT3 at Tyr705 but not Ser727 (Figure 4G-H). Also, IH exposure or together with Ang II markedly increased STAT3 nuclear localization *in vivo* (Figure 4I). Thus, IH induced STAT3 activation via JAK2-mediated STAT3 phosphorylation at Tyr705.

STAT3 silencing or inhibition blunted IH-induced TSP1 expression and CF activation.

We next explored the role of STAT3 in IH-induced TSP1 expression and CF activation. Knockdown of STAT3 with siRNA almost completely abolished IH induced TSP1 expression both in mRNA and protein level (Figure 5A-C). Simultaneously, IH-induced α -SMA, collagen I and periostin expression was blocked by STAT3 knockdown at both the mRNA and protein level (Figure 5A-C). To further assess the importance of STAT3 transcriptional activity, we treated PCFs with S3I-201, a selective STAT3 inhibitor. S3I-201 barely showed effect on the basal level of TSP1, α -SMA, collagen I and periostin expression but significantly attenuated IH-induced expression of TSP1, α -SMA, collagen I and periostin at both the mRNA and protein level (Figure 5D-F). Quantitative chromatin immunoprecipitation (ChIP) assay proved that IH enhanced the enrichment of STAT3 at TSP1 promoter in PCFs as compared with the control (Figure 5-figure supplement 1A). Taken together, our results indicated a predominant

role of STAT3 in IH-induced CF activation.

Pharmacological or genetic inhibition of STAT3 ameliorates IH-induced cardiac dysfunction and fibrosis.

As we found that STAT3-induced TSP1 contributed to IH-induced CF activation, we injected S3I-201 into IH-exposed mice with or without Ang II infusion for 28 days (Figure 6A). First, echocardiography analysis showed that S3I-201 promoted significant recovery of ratio of heart weight to tibial length (Figure 6B) and EF after IH exposure (Figure 6C). Moreover, on Masson staining, S3I-201 reduced IH-induced fibrosis under both basal and Ang II infusion conditions (Figure 6D-E). In addition, immunofluorescence staining showed significantly decreased TSP1, collagen I, periostin and α -SMA expression in the mouse left ventricle after S3I-201 treatment under both basal and Ang II infusion conditions (Figure 6D-E). The expression of TSP1, collagen I, periostin and α -SMA, as well as phosphorylation of STAT3 at Tyr705 site in the left ventricle showed similar trends (Figure 6F-G).

To further investigate whether S3I-201 could reverse the damage already induced by IH, we treated mice with S3I-201 for 2 weeks after exposure to IH and Ang II for 28 days (Figure 6-figure supplement 1A). The ratio of heart weight to tibial length, EF and fibrotic area in mice were comparable between groups (Figure 6-figure supplement 1B-E). In addition, because systemic S3I-201 administration might protect the heart via direct and indirect mechanisms, we determined the effect of AAV9-periostin promoter-shStat3 on IH-induced fibrosis (Figure 6-figure supplement 1F). Evidence from flow cytometry confirmed the knockdown of STAT3 in CFs (Figure 6-figure supplement 1G). Similar to that observed in animals subjected to S3I-201 treatment, AAV9-periostin promoter-shStat3 promoted a significant recovery of ratio of heart weight to tibial length and EF after IH exposure (Figure 6-figure supplement 1H-I), and reduced IH-induced fibrosis under both basal and Ang II infusion conditions (Figure 6-figure supplement 1J-K). These results suggest that pharmacological or genetic inhibition of STAT3 might be a potential therapeutic strategy for

206 Discussion

207 In the last decades, we have extensive evidence for a causal link between OSA and
208 cardiovascular disease²⁵. Here, we provide definitive evidence of elevated plasma TSP1 level
209 in both humans with OSA and mice exposed to IH. Moreover, we found that TSP1 activated
210 TGF β signaling, which subsequently promoted the transformation of CFs to myofibroblasts,
211 dependent on STAT3 Tyr705 phosphorylation. Finally, pharmacological inhibition of STAT3
212 with S3I-201 or AAV9-periostin promoter-shStat3 significantly attenuated IH-induced cardiac
213 fibrosis under both basal and Ang II infusion conditions (Figure 6H).

214 TSP1 belongs to the thrombospondin family, a conserved family of extracellular, oligomeric,
215 multidomain, calcium-binding glycoproteins that can be secreted by various cell types^{9, 10, 26}.
216 Increased TSP1 levels are associated with many kinds of cardiovascular diseases, including
217 pulmonary hypertension (PH), idiopathic interstitial pneumonia and aging²⁷⁻³¹. In individuals
218 with end-stage PH, both protein and mRNA levels of TSP1 are elevated in the lung
219 parenchyma and pulmonary artery³¹. Furthermore, TSP1 blockade protected against
220 Schistosoma- and hypoxia-induced PH³⁰. In our study, TSP1 protein expression was
221 significantly elevated in patients with OSA as compared with healthy controls. Strikingly,
222 OSA incidence is high in patients with PH, idiopathic pulmonary fibrosis, and other cardiac
223 diseases, which suggests that TSP1 might be the common pathologic mechanism in
224 OSA-associated cardiovascular diseases. Therefore, TSP1 might be a biomarker for diagnosis
225 of OSA-related cardiac dysfunction, and reducing IH-upregulated TSP1 expression might be
226 crucial to protect the cardiac function of patients with sleep apnea.

227 TGF β , perhaps the most extensively studied mediator of fibroblast activation and having the
228 greatest role in pathological fibrosis^{7, 32}, can be activated by TSP1 binding to a defined site on
229 latency-associated propeptide and inducing a conformational change in the latent complex^{33, 34}.
230 The kinetics of its gene expression, along with its independence from de novo protein
231 synthesis, led to classifying TSP1 as an immediate early-response gene^{35, 36}. For example, in

vascular smooth muscle cells, the mRNA level of TSP1 was induced rapidly within 15 min by platelet-derived growth factor³⁵. Consistently, we found that IH upregulated *Thbs1* continuously from 2 to 8 hr. However, IH-induced TSP1 protein expression in PCFs peaked at 2 hr and decreased from 4 to 8 hr. The concentration of TSP1 in culture medium was still increased from 4 to 8 hr, which suggests that IH might promote TSP1 secretion as well. However, the mechanism underlying TSP1 secretion needs further elucidation.

STAT3, as a multifaceted molecule, plays a central role in organic fibrogenesis and cardiac hypertrophy¹⁶. Hypoxic stress can induce phosphorylation of STAT3 and its simultaneous nuclear translocation³⁷. Here we found that STAT3, as a TSP1 transcription factor, was phosphorylated at Tyr705 and translocated into the nucleus after IH exposure, then promoted fibroblast activation. In addition, STAT3-null mice showed severe fibrosis with age³⁸, but in transaortic constriction-induced cardiac remodeling, selective inhibition of STAT3 by S3I-201 significantly improved EF and decreased the left ventricle chamber dilation³⁹. Consistently, we found that S3I-201 treatment reduced the pathologic upregulation of TSP1 and ameliorated the cardiac fibrosis of IH-exposed mice with or without Ang II infusion. Importantly, these results were further confirmed by using AAV9-periostin promoter-shStat3. Direct blockade of TSP1/TGF β signaling is a major therapeutic challenge because of its ubiquitous nature and localized signaling effects³⁰. Our results indicated that targeting the pathologic activation of STAT3 might hold promise as a potentially safe approach in preventing IH-induced cardiac fibrosis.

In summary, our study demonstrated that IH upregulated the expression of TSP1 in both mice and humans, and TGF β pathway activation induced by JAK2/STAT3/TSP1 signaling played a vital role in IH-induced fibroblast activation and cardiac fibrosis. Pharmacological or genetic inhibition of STAT3 might be a potential therapeutic strategy in managing several diverse yet intertwined human pathologies related to IH.

Key Resources Table				
Reagent type (species) or resource	Designation	Source or reference	Identifiers	Additional information
antibody	anti-thrombospondin-1 (Rabbit monoclonal)	Cell Signaling Technology	Cat# 37879	WB (1:1000)
antibody	anti-phospho-SMAD2/3 (Rabbit monoclonal)	Cell Signaling Technology	Cat# 8828	WB (1:1000)
antibody	anti-SMAD2/3 (Rabbit monoclonal)	Cell Signaling Technology	Cat# 8685	WB (1:1000)
antibody	anti-phospho-JAK1 (Rabbit monoclonal)	Cell Signaling Technology	Cat# 74129	WB (1:1000)
antibody	anti-phospho-JAK2 (Rabbit monoclonal)	Cell Signaling Technology	Cat# 8082	WB (1:1000)
antibody	anti-phospho-JAK3 (Rabbit monoclonal)	Cell Signaling Technology	Cat# 5031	WB (1:1000)
antibody	anti-JAK1 (Rabbit monoclonal)	Cell Signaling Technology	Cat# 3344	WB (1:1000)
antibody	anti-JAK2 (Rabbit monoclonal)	Cell Signaling Technology	Cat# 3230	WB (1:1000)
antibody	anti-JAK3 (Rabbit monoclonal)	Cell Signaling Technology	Cat# 8827	WB (1:1000)

antibody	anti-phospho-S TAT3(Tyr705) (Rabbit monoclonal)	Cell Signaling Technology	Cat# 9145,	WB (1:1000)
antibody	anti-phospho-S TAT3(Ser727) (Rabbit polyclonal)	Cell Signaling Technology	Cat# 9134	WB (1:1000)
antibody	anti-STAT3 (Rabbit monoclonal)	Cell Signaling Technology	Cat# 12640	WB (1:1000) ChIP (1:50)
antibody	anti-STAT3 (Mouse monoclonal)	Cell Signaling Technology	Cat# 9139	IF (1:100) FACS (1 μ L per test)
antibody	Normal Rabbit IgG	Cell Signaling Technology	Cat# 2729	ChIP (1 μ g per test)
antibody	anti-thrombosp ondin antibody (Mouse monoclonal)	Abcam	Cat# ab1823	IF (1:50) FACS (1 μ L per test)
antibody	anti- α SMA (Mouse monoclonal)	Abcam	Cat# ab7817	WB (1:1000) IF (1:100)
antibody	anti-Collagen I antibody (Mouse monoclonal)	Abcam	Cat# ab6308	WB (1:1000) IF (1:100)
antibody	anti-periostin (Rabbit polyclonal)	Abcam	Cat# ab14041	WB (1:1000) IF (1:100)
antibody	anti-vimentin (Rabbit monoclonal)	Abcam	Cat# ab92547	IF (1:500)
antibody	anti-GAPDH (Mouse monoclonal)	Proteintech	Cat# 60004	WB (1:1000)

antibody	anti-Ki67 (Rabbit monoclonal)	HuaAn Biotechnology Co	Cat# ET1609-34	IF (1:100)
antibody	anti-mouse CD45-PE Cy7 (Rat monoclonal)	BioLegend	Cat# 103114	FACS (1 µL per test)
antibody	anti-mouse CD31-PE Cy7 (Rat monoclonal)	BioLegend	Cat# 102523	FACS (1 µL per test)
antibody	anti-mouse CD11b-PE Cy7 (Rat monoclonal)	BioLegend	Cat# 101215	FACS (1 µL per test)
antibody	anti-mouse Ter119-PE Cy7 (Rat monoclonal)	BioLegend	Cat# 116221	FACS (1 µL per test)
antibody	anti-mouse thyl- Alexa Fluor® 488 (Mouse monoclonal)	BioLegend	Cat# 202505	FACS (1 µL per test)
antibody	anti-mouse thyl- Alexa Fluor® 488 (Rat monoclonal)	BioLegend	Cat# 105315	FACS (1 µL per test)
antibody	PE RAT anti-mouse IgG1	BD Biosciences	Cat# 550083	FACS (1 µL per test)
antibody	Alex 594-conjugated goat anti-mouse antibody	Thermo Fisher Scientific	Cat# A-11005	IF (1:200)

antibody	Alex 488-conjugated goat anti-rabbit antibody	Thermo Fisher Scientific	Cat# A-11008	IF (1:200)
sequence-based reagent	Stat3 siRNA	Santa Cruz Biotechnology	Cat# sc-29494	
sequence-based reagent	Control siRNA	Santa Cruz Biotechnology	Cat# sc-37007	
sequence-based reagent	Mouse Acta	This paper	N/A	Sequences in Supplemental file 1
sequence-based reagent	Mouse Colla1	This paper	N/A	Sequences in Supplemental file 1
sequence-based reagent	Mouse Postn	This paper	N/A	Sequences in Supplemental file 1
sequence-based reagent	Mouse Thbs1	This paper	N/A	Sequences in Supplemental file 1
sequence-based reagent	Mouse Tnfa	This paper	N/A	Sequences in Supplemental file 1
sequence-based reagent	Mouse Stat3	This paper	N/A	Sequences in Supplemental file 1
sequence-based reagent	Mouse 18S	This paper	N/A	Sequences in Supplemental file 1

peptide, recombinant protein	Angiotensin II	Abcam	Cat# ab120183	
commercial assay or kit	TSP1 ELISA KIT(Human)	R&D Systems	Cat# DTSP10	
commercial assay or kit	TSP1 ELISA KIT(Mouse)	Cloud-Clone Corp.	Cat# SEA611Mu	
commercial assay or kit	TUNEL staining kit	KeyGEN BioTECH	Cat# KGA7073-1	
commercial assay or kit	SimpleChIP® Enzymatic Chromatin IP Kit	Cell Signaling Technology	Cat# 9003	
commercial assay or kit	Eastep® Super Total RNA Extraction Kit	Promega Corporation	Cat# LS1040	
chemical compound, drug	S3I-201	Santa Cruz Biotechnology	Cat# sc-204304	
chemical compound, drug	TG101209	MedChem Express	Cat# HY-10410	
software, algorithm	Prism version 7.0	GraphPad Software Inc	https://www.graphpad.com/scientific-software/prism/	
software, algorithm	ImageJ version 1.52a	NIH	https://imagej.nih.gov/ij/	
software, algorithm	FlowJo version 10	Tree Star Inc	https://www.flowjo.com/solutions/flowjo/downloads	

Male C57BL/6J mice at 8-10 weeks of age were used. All mice were housed in a controlled environment ($20 \pm 2^{\circ}\text{C}$, 12-hr/12-hr light/dark cycle) and maintained on a standard chow diet with free access to water. Intermittent hypoxia (IH) was induced as described previously by using an automated system to control ambient oxygen concentration^{40, 41}. Briefly, O_2 concentration was decreased to 4–6% approximately every 60 sec. IH mice were exposed to IH for 8 hr/day in the light time for 28 days. In the pathologic cardiac fibrosis model, mice were subcutaneously implanted with an osmotic minipump (2004 model, Alzet, CA) containing Ang II (1 mg/kg/day) in saline (0.9% w/v) or an identical volume of saline. After the surgery, all mice were exposed to IH for 28 days. In rescue experiments, S3I-201 (5 mg/kg) was given by intraperitoneal injection every 2 days during or after the IH exposure.

Adeno-associated virus (AAV) construction and infection

The AAV used in this study was constructed as previously reported⁴². Briefly, AAV9 carrying a periostin promoter driving the expression of shRNA targeting Stat3 (AAV9-periostin promoter-shStat3) was constructed by Shanghai Genechem Co. (Shanghai). The sequences of the shRNAs were for shStat3, GTCACACAGATGAACTTGGTCTTCAGGT and GCATCAATCCTGTGGTATA. The periostin AAV9-periostin promoter-shStat3 or AAV9-periostin promoter-shScramble (1.5×10^{11} v.g) was injected into the tail vein of mice. At 1-week post-injection, mice were exposed to IH with or without Ang II infusion.

Echocardiography

Trans-thoracic echocardiography was performed on all mice by using a Vevo 2100 system with a MS400 linear array transducer (VisualSonics, ON, Canada) as previously reported⁴³. Briefly, mice were anesthetized with 2% isoflurane and kept warm on a heated platform (37°C). The chest hairs were removed by using depilatory cream, and a layer of acoustic coupling gel was applied to the thorax. An average of 10 cardiac cycles of standard 2-D and m-mode short axis at mid-papillary muscle level were analyzed. Left ventricular ejection fraction and dimensions were calculated by using a modified Quinone method.

Histology

Tissues were fixed in 10% neutral-buffered formalin for 24 hr at room temperature and embedded in paraffin. Hearts were sectioned at $5\text{ }\mu\text{m}$ for staining. Collagen deposition was stained with Masson's trichrome (Sigma-Aldrich, MO) and Sirius red (Solarbio Life Sciences,

Beijing) according to the manufacturer's instructions. Images of sections were captured under an Olympus inverted microscope (IX53, Tokyo) and fibrotic areas were semi-quantitatively determined by using ImageJ 1.52.

For immunofluorescence staining, harvested hearts were fixed and embedded in OCT (VWR, PA) and sectioned at 5 μ m. Then, sections were stained with primary antibodies for TSP1, Collagen I, periostin, α -SMA and vimentin overnight at 4°C. Alex 488-conjugated goat anti-rabbit and Alex 594-conjugated goat anti-mouse antibodies were used as secondary antibodies. Nuclei were stained with DAPI. TUNEL staining kit (KGA7073-1, KeyGEN BioTECH, Nanjing) was used for analyzing apoptotic cells in cardiac tissue. Images were acquired under an Olympus inverted microscope (IX81, Tokyo). Fluorescent intensity was quantified by using ImageJ. Colocalization of α -SMA and vimentin was quantified by using the Image J with colocalization plugin. Briefly, the plugin initially generates an 8-bit image with only the colocalized points, then it combines the three 8-bit images in an RGB image. Two points are considered as colocalized if their respective intensities are strictly higher than the threshold of their channels.

RT-qPCR

RNA was extracted by using the Eastep Super Total RNA Extraction Kit (LS1040, Promega, WI). cDNA was synthesized by using the iScript cDNA Synthesis Kit (Bio-Rad, CA). Quantitative RT-PCR was performed with gene-specific primers shown in Supplementary file 1.

Western blot analysis

Proteins were isolated from snap-frozen heart tissue and cultured cardiac fibroblasts (CFs), which were extracted in RIPA solution with a protease inhibitor cocktail (#4693132001) and PhosSTOP (#04906845001, both Roche, IN). Proteins were quantified by using the BCA Protein Assay Kit (Thermo Fisher Scientific, MA). Then, 20 μ g each protein was separated on SDS-PAGE and electrotransferred onto PVDF membranes, blocked with TBST containing 5% bovine serum albumin, and blots on membranes incubated with antigen and antibody complexes were detected by an ECL protocol with horseradish peroxidase-conjugated IgG as secondary antibodies. Immunoblots were quantified by using ImageJ 1.52.

Isolation and culture of primary CFs (PCFs)

Isolation of mouse primary CFs (mPCFs) was performed as previously reported¹⁶. Briefly, mouse hearts from freshly euthanized C57BL/6 mice were harvested and minced to 1 mm³ in cold phosphate buffered saline. Minced tissue was subsequently digested with buffer containing collagenase II (#V900892, Sigma-Aldrich, MO) and trypsin (Solarbio life Sciences, Beijing) under constant stirring at 37 °C for 60 min. The supernatants were spun to collect cells. Then cells resuspended in DMEM/F12 (#11320033, Gibco, MA) were plated into dishes and incubated for 2 hr. Supernatant was discarded and dishes were replenished with fresh medium. mPCFs were incubated at 37 °C in a humidified atmosphere of 5% CO₂ and grown to 70–80% confluence. Cells at passages 2 to 3 were used in experiments. Cells exposed to IH were maintained in a hypoxia chamber (5% CO₂; balance N₂ and O₂ from 5% to 21%) for the indicated times.

Flow cytometry

Flow cytometry was performed as previously reported²⁰. Digested cells from mouse hearts were suspended in staining buffer containing the relevant surface marker antibodies (PE/Cy7 anti-mouse CD45, CD31, CD11b, Ter119, and Alexa Fluor® 488 anti-mouse Thy1) in the dark for 30 min at room temperature. Then, for intracellular staining, cells were fixed with cold methanol for 10 min at -20°C, then incubated with a stain buffer containing TSP1 or STAT3 antibody. After three washing steps, a secondary antibody conjugated to PE was added. The cells were then washed and ready for analysis.

Cell immunofluorescence staining

Mouse primary CFs were fixed with 4% paraformaldehyde and permeabilized with 0.25% Triton X-100. Then cells were stained with antibodies against α -SMA (1:100), STAT3 (1:100) or Ki67 (1:100). Alexa Fluor antibodies (1:200) were used as secondary antibodies. Stress fibers were stained with rhodamine phalloidin (Thermo Fisher Scientific, MA). Nuclei were stained with DAPI. Images were acquired under an Olympus laser scanning microscope (IX81, Tokyo).

Collagen gel contraction assay

The collagen contraction assay was performed as previously reported⁴⁴. Mouse primary CFs were embedded in collagen gel containing collagen type I from rat tail (#08-115, Sigma-Aldrich, MO) and culture medium. Contraction was measured from the gel images

350 after 24 hr.

351 **Lentivirus construction and infection**

352 Lentiviruses carrying short hairpin (shRNA) for *Thbs1* (LV-shThbs1) and non-specific shRNA
353 (LV-shCtrl) were constructed by Shanghai Genechem Co. (Shanghai). CFs were infected with
354 lentivirus at multiplicity of infection (MOI) 10, and no detectable cellular toxicity was
355 observed.

356 **ELISA**

357 The secretion of TSP1 in mice or human plasma was quantified by using an ELISA kit
358 (SEA611Mu, Cloud-Clone Corp., TX and DTSP10 R&D Systems, MN) according to the
359 manufacturer's instructions.

360 **siRNA transfection**

361 Mouse primary CFs were seeded on plates and cultured to 80% confluence, then transfected
362 with Stat3 siRNA (#sc-29494) or control siRNA (#sc-37007, both Santa Cruz Biotechnology,
363 CA) by using Lipofectamine RNAi MAX transfection reagent (Thermo Fisher Scientific, MA)
364 for 24 hr.

365 **Chromatin immunoprecipitation (ChIP) assay**

366 ChIP was performed as previously reported¹⁵ with SimpleChIP® Enzymatic Chromatin IP
367 Kits (Cell Signaling Technology, MA) according to the manufacturer's instructions. Briefly,
368 mPCFs were crosslinked with 1% formaldehyde followed by quenching with glycine for 5
369 min. Cell lysates were digested by micrococcal nuclease, sonicated, and proteins were
370 immunoprecipitated with antibody to STAT3 or rabbit IgG as a control. After complete
371 washing, immunoprecipitated DNA was eluted with elution buffer and reverse-crosslinked
372 overnight at 65 °C. DNA was purified and quantified by quantitative RT-PCR. Enrichment
373 was calculated relative to input. Primers for ChIP-qPCR were forward, 5'-
374 TGGCTTCCTCTGTGGTCTCT-3', and reverse, 5'-GTCAAGGTCATGGGATGGTC-3'.

375 **Statistical analysis**

376 Sample sizes were designed with adequate power according to the literature and our previous
377 studies. Data are presented as mean ± standard error of the mean (SEM). Statistical analysis
378 involved use of GraphPad Prism 7 v7.04 with two-tailed, unpaired Student's *t* test or one-way
379 or two-way ANOVA with Bonferroni multiple comparison post-test, as appropriate. The

380 criterion for statistical significance was $P < 0.05$.

381

382 **Acknowledgements**

383 This work was supported by grants from the National Natural Science Foundation of China
384 (81800251, 81570304, 81800297).

385 **Ethics**

386 Ethical approval was obtained through the institutional ethical review board of Peking
387 University People's Hospital (Permit Number: 2018PHB210-01). The study was conducted in
388 accordance with the Declaration of Helsinki. Written informed consent was taken from all
389 study participants. Animal procedures were approved and conducted in accordance with the
390 Experimental Animal Administration Committee of Tianjin Medical University (Permit
391 Number: SYXK 2011-0006; SYXK 2016-0012).

392 **Competing interests**

393 None.

- 395 1. Javaheri S, Barbe F, Campos-Rodriguez F, Dempsey JA, Khayat R, Javaheri S, Malhotra
396 A, Martinez-Garcia MA, Mehra R, Pack AI, Polotsky VY, Redline S and Somers VK. Sleep
397 Apnea: Types, Mechanisms, and Clinical Cardiovascular Consequences. *J Am Coll Cardiol*.
398 2017;69:841-858.
- 399 2. Kasai T, Floras JS and Bradley TD. Sleep apnea and cardiovascular disease: a
400 bidirectional relationship. *Circulation*. 2012;126:1495-510.
- 401 3. Somers VK, White DP, Amin R, Abraham WT, Costa F, Culebras A, Daniels S, Floras JS,
402 Hunt CE, Olson LJ, Pickering TG, Russell R, Woo M, Young T, American Heart Association
403 Council for High Blood Pressure Research Professional Education Committee CoCC,
404 American Heart Association Stroke C, American Heart Association Council on
405 Cardiovascular N and American College of Cardiology F. Sleep apnea and cardiovascular
406 disease: an American Heart Association/american College Of Cardiology Foundation
407 Scientific Statement from the American Heart Association Council for High Blood Pressure
408 Research Professional Education Committee, Council on Clinical Cardiology, Stroke Council,
409 and Council On Cardiovascular Nursing. In collaboration with the National Heart, Lung, and
410 Blood Institute National Center on Sleep Disorders Research (National Institutes of Health).
411 *Circulation*. 2008;118:1080-111.
- 412 4. Gottlieb DJ, Yenokyan G, Newman AB, O'Connor GT, Punjabi NM, Quan SF, Redline S,
413 Resnick HE, Tong EK, Diener-West M and Shahar E. Prospective study of obstructive sleep
414 apnea and incident coronary heart disease and heart failure: the sleep heart health study.
415 *Circulation*. 2010;122:352-60.
- 416 5. Baguet JP, Barone-Rochette G, Tamisier R, Levy P and Pepin JL. Mechanisms of cardiac
417 dysfunction in obstructive sleep apnea. *Nat Rev Cardiol*. 2012;9:679-88.
- 418 6. Wei Q, Bian Y, Yu F, Zhang Q, Zhang G, Li Y, Song S, Ren X and Tong J. Chronic
419 intermittent hypoxia induces cardiac inflammation and dysfunction in a rat obstructive sleep
420 apnea model. *J Biomed Res*. 2016;30:490-495.
- 421 7. Travers JG, Kamal FA, Robbins J, Yutzey KE and Blaxall BC. Cardiac Fibrosis: The
422 Fibroblast Awakens. *Circ Res*. 2016;118:1021-40.
- 423 8. Meng XM, Nikolic-Paterson DJ and Lan HY. TGF-beta: the master regulator of fibrosis.
424 *Nat Rev Nephrol*. 2016;12:325-38.
- 425 9. Crawford SE, Stellmach V, Murphy-Ullrich JE, Ribeiro SM, Lawler J, Hynes RO, Boivin
426 GP and Bouck N. Thrombospondin-1 is a major activator of TGF-beta1 in vivo. *Cell*.
427 1998;93:1159-70.
- 428 10. Adams JC and Lawler J. The thrombospondins. *Cold Spring Harb Perspect Biol*.
429 2011;3:a009712.
- 430 11. Xia Y, Dobaczewski M, Gonzalez-Quesada C, Chen W, Biernacka A, Li N, Lee DW and
431 Frangogiannis NG. Endogenous thrombospondin 1 protects the pressure-overloaded
432 myocardium by modulating fibroblast phenotype and matrix metabolism. *Hypertension*.
433 2011;58:902-11.
- 434 12. Belmadani S, Bernal J, Wei CC, Pallero MA, Dell'italia L, Murphy-Ullrich JE and
435 Berecek KH. A thrombospondin-1 antagonist of transforming growth factor-beta activation
436 blocks cardiomyopathy in rats with diabetes and elevated angiotensin II. *Am J Pathol*.

2007;171:777-89.

13. Wei LH, Kuo ML, Chen CA, Chou CH, Lai KB, Lee CN and Hsieh CY. Interleukin-6 promotes cervical tumor growth by VEGF-dependent angiogenesis via a STAT3 pathway. *Oncogene*. 2003;22:1517-27.

14. Chakraborty D, Sumova B, Mallano T, Chen CW, Distler A, Bergmann C, Ludolph I, Horch RE, Gelse K, Ramming A, Distler O, Schett G, Senolt L and Distler JHW. Activation of STAT3 integrates common profibrotic pathways to promote fibroblast activation and tissue fibrosis. *Nat Commun*. 2017;8:1130.

15. He J, Bao Q, Zhang Y, Liu M, Lv H, Liu Y, Yao L, Li B, Zhang C, He S, Zhai G, Zhu Y, Liu X, Zhang K, Wang XJ, Zou MH, Zhu Y and Ai D. Yes-Associated Protein Promotes Angiogenesis via Signal Transducer and Activator of Transcription 3 in Endothelial Cells. *Circ Res*. 2018;122:591-605.

16. Su SA, Yang D, Wu Y, Xie Y, Zhu W, Cai Z, Shen J, Fu Z, Wang Y, Jia L, Wang Y, Wang JA and Xiang M. EphrinB2 Regulates Cardiac Fibrosis Through Modulating the Interaction of Stat3 and TGF-beta/Smad3 Signaling. *Circ Res*. 2017;121:617-627.

17. Tyzack GE, Sitnikov S, Barson D, Adams-Carr KL, Lau NK, Kwok JC, Zhao C, Franklin RJ, Karadottir RT, Fawcett JW and Lakatos A. Astrocyte response to motor neuron injury promotes structural synaptic plasticity via STAT3-regulated TSP-1 expression. *Nat Commun*. 2014;5:4294.

18. Schafer S, Viswanathan S, Widjaja AA, Lim W-W, Moreno-Moral A, DeLaughter DM, Ng B, Patone G, Chow K, Khin E, Tan J, Chothani SP, Ye L, Rackham OJL, Ko NSJ, Sahib NE, Pua CJ, Zhen NTG, Xie C, Wang M, Maatz H, Lim S, Saar K, Blachut S, Petretto E, Schmidt S, Putoczki T, Guimarães-Camboa N, Wakimoto H, van Heesch S, Sigmundsson K, Lim SL, Soon JL, Chao VTT, Chua YL, Tan TE, Evans SM, Loh YJ, Jamal MH, Ong KK, Chua KC, Ong B-H, Chakaramakkil MJ, Seidman JG, Seidman CE, Hubner N, Sin KYK and Cook SA. IL-11 is a crucial determinant of cardiovascular fibrosis. *Nature*. 2017;552:110.

19. Cucoranu I, Clempus R, Dikalova A, Phelan PJ, Ariyan S, Dikalov S and Sorescu D. NAD(P)H oxidase 4 mediates transforming growth factor-beta1-induced differentiation of cardiac fibroblasts into myofibroblasts. *Circ Res*. 2005;97:900-7.

20. Ali SR, Ranjbarvaziri S, Talkhabi M, Zhao P, Subat A, Hojjat A, Kamran P, Muller AM, Volz KS, Tang Z, Red-Horse K and Ardehali R. Developmental heterogeneity of cardiac fibroblasts does not predict pathological proliferation and activation. *Circ Res*. 2014;115:625-35.

21. Hudon-David F, Bouzeghrane F, Couture P and Thibault G. Thy-1 expression by cardiac fibroblasts: lack of association with myofibroblast contractile markers. *J Mol Cell Cardiol*. 2007;42:991-1000.

22. Wang Z, Li J, Xiao W, Long J and Zhang H. The STAT3 inhibitor S3I-201 suppresses fibrogenesis and angiogenesis in liver fibrosis. *Lab Invest*. 2018;98:1600-1613.

23. Darnell JE, Jr., Kerr IM and Stark GR. Jak-STAT pathways and transcriptional activation in response to IFNs and other extracellular signaling proteins. *Science*. 1994;264:1415-21.

24. Ihle JN. Cytokine receptor signalling. *Nature*. 1995;377:591-4.

25. Gozal D and Kheirandish-Gozal L. Cardiovascular morbidity in obstructive sleep apnea: oxidative stress, inflammation, and much more. *Am J Respir Crit Care Med*. 2008;177:369-75.

26. Hugo C, Shankland SJ, Pichler RH, Couser WG and Johnson RJ. Thrombospondin 1 precedes and predicts the development of tubulointerstitial fibrosis in glomerular disease in the rat. *Kidney Int.* 1998;53:302-11.
27. Ide M, Ishii H, Mukae H, Iwata A, Sakamoto N, Kadota J and Kohno S. High serum levels of thrombospondin-1 in patients with idiopathic interstitial pneumonia. *Respir Med.* 2008;102:1625-30.
28. van Almen GC, Verhesen W, van Leeuwen RE, van de Vrie M, Eurlings C, Schellings MW, Swinnen M, Cleutjens JP, van Zandvoort MA, Heymans S and Schroen B. MicroRNA-18 and microRNA-19 regulate CTGF and TSP-1 expression in age-related heart failure. *Aging Cell.* 2011;10:769-79.
29. Kaiser R, Frantz C, Bals R and Wilkens H. The role of circulating thrombospondin-1 in patients with precapillary pulmonary hypertension. *Respir Res.* 2016;17:96.
30. Kumar R, Mickael C, Kassa B, Gebreab L, Robinson JC, Koyanagi DE, Sanders L, Barthel L, Meadows C, Fox D, Irwin D, Li M, McKeon BA, Riddle S, Dale Brown R, Morgan LE, Evans CM, Hernandez-Saavedra D, Bandeira A, Maloney JP, Bull TM, Janssen WJ, Stenmark KR, Tudor RM and Graham BB. TGF-beta activation by bone marrow-derived thrombospondin-1 causes Schistosoma- and hypoxia-induced pulmonary hypertension. *Nat Commun.* 2017;8:15494.
31. Rogers NM, Sharifi-Sanjani M, Yao M, Ghimire K, Bienes-Martinez R, Mutchler SM, Knupp HE, Baust J, Novelli EM, Ross M, St Croix C, Kuttan JC, Czajka CA, Sembrat JC, Rojas M, Labrousse-Arias D, Bachman TN, Vanderpool RR, Zuckerbraun BS, Champion HC, Mora AL, Straub AC, Bilonick RA, Calzada MJ and Isenberg JS. TSP1-CD47 signaling is upregulated in clinical pulmonary hypertension and contributes to pulmonary arterial vasculopathy and dysfunction. *Cardiovasc Res.* 2017;113:15-29.
32. Leask A and Abraham DJ. TGF-beta signaling and the fibrotic response. *FASEB J.* 2004;18:816-27.
33. Murphy-Ullrich JE and Poczatek M. Activation of latent TGF-beta by thrombospondin-1: mechanisms and physiology. *Cytokine Growth Factor Rev.* 2000;11:59-69.
34. Ribeiro SM, Poczatek M, Schultz-Cherry S, Villain M and Murphy-Ullrich JE. The activation sequence of thrombospondin-1 interacts with the latency-associated peptide to regulate activation of latent transforming growth factor-beta. *J Biol Chem.* 1999;274:13586-93.
35. Majack RA, Mildbrandt J and Dixit VM. Induction of thrombospondin messenger RNA levels occurs as an immediate primary response to platelet-derived growth factor. *J Biol Chem.* 1987;262:8821-5.
36. Patel MK, Lymn JS, Clunn GF and Hughes AD. Thrombospondin-1 is a potent mitogen and chemoattractant for human vascular smooth muscle cells. *Arterioscler Thromb Vasc Biol.* 1997;17:2107-14.
37. Noman MZ, Buart S, Van Pelt J, Richon C, Hasmim M, Leleu N, Suchorska WM, Jalil A, Lecluse Y, El Hage F, Giuliani M, Pichon C, Azzarone B, Mazure N, Romero P, Mami-Chouaib F and Chouaib S. The cooperative induction of hypoxia-inducible factor-1 alpha and STAT3 during hypoxia induced an impairment of tumor susceptibility to CTL-mediated cell lysis. *J Immunol.* 2009;182:3510-21.
38. Jacoby JJ, Kalinowski A, Liu MG, Zhang SS, Gao Q, Chai GX, Ji L, Iwamoto Y, Li E,

Schneider M, Russell KS and Fu XY. Cardiomyocyte-restricted knockout of STAT3 results in higher sensitivity to inflammation, cardiac fibrosis, and heart failure with advanced age. *Proc Natl Acad Sci U S A*. 2003;100:12929-34.

39. Unudurthi SD, Nassal D, Greer-Short A, Patel N, Howard T, Xu X, Onal B, Satroplus T, Hong D, Lane C, Dalic A, Koenig SN, Lehnig AC, Baer LA, Musa H, Stanford KI, Smith S, Mohler PJ and Hund TJ. betaIV-Spectrin regulates STAT3 targeting to tune cardiac response to pressure overload. *J Clin Invest*. 2018;128:5561-5572.

40. Savransky V, Nanayakkara A, Li J, Bevans S, Smith PL, Rodriguez A and Polotsky VY. Chronic intermittent hypoxia induces atherosclerosis. *Am J Respir Crit Care Med*. 2007;175:1290-7.

41. Chen L, Einbinder E, Zhang Q, Hasday J, Balke CW and Scharf SM. Oxidative stress and left ventricular function with chronic intermittent hypoxia in rats. *Am J Respir Crit Care Med*. 2005;172:915-20.

42. Piras BA, Tian Y, Xu Y, Thomas NA, O'Connor DM and French BA. Systemic injection of AAV9 carrying a periostin promoter targets gene expression to a myofibroblast-like lineage in mouse hearts after reperfused myocardial infarction. *Gene Ther*. 2016;23:469-78.

43. Zhang K, Zhao L, Ma Z, Wang W, Li X, Zhang Y, Yuan M, Liang X and Li G. Doxycycline Attenuates Atrial Remodeling by Interfering with MicroRNA-21 and Downstream Phosphatase and Tensin Homolog (PTEN)/Phosphoinositide 3-Kinase (PI3K) Signaling Pathway. *Med Sci Monit*. 2018;24:5580-5587.

44. Pincha N, Hajam EY, Badarinath K, Batta SPR, Masudi T, Dey R, Andreasen P, Kawakami T, Samuel R, George R, Danda D, Jacob PM and Jamora C. PAI1 mediates fibroblast-mast cell interactions in skin fibrosis. *J Clin Invest*. 2018;128:1807-1819.

549 **Figure legends**

550 **Figure 1. Intermittent hypoxia (IH) induces cardiac fibrosis and aggravates pathological**
551 **cardiac dysfunction by promoting fibroblast activation in myocardial interstitium.**

552 **A)** C57BL/6 mice were housed under normoxia or IH with or without infusion of angiotensin
553 II (Ang II) for 28 days. **B)** Ratio of heart weight to tibial length of mice in each group. **C, D)**
554 Ejection fraction (EF) and fractional shortening (FS) of mice quantified by echocardiography.
555 **E)** Representative images of Masson and Sirius red staining of left ventricle. Scale bar, 100
556 μm . **F)** Quantification of fibrotic area in (E). **G)** Representative confocal microscopy images
557 of immunofluorescence staining for α -SMA, vimentin (VIME, fibroblast marker), collagen I
558 (Col1), periostin and DAPI. Scale bar, 20 μm . **H)** Quantification of co-localization of α -SMA
559 and VIME, collagen I and periostin fluorescence intensity in (G). **I)** Col1, periostin, and
560 α -SMA protein level in left ventricle detected by western blot analysis. **J)** Quantification of
561 Col1, periostin and α -SMA protein level in (I). **K)** Quantification of *Acta2*, *colla1* and *Postn*
562 mRNA expression. Data are mean \pm SEM, n=6 mice per group, *P<0.05, 2-way ANOVA with
563 Bonferroni post-test. Data used for quantitative analyses as well as the numerical data that are
564 represented in graphs are available in Figure 1-source data.

565 **Figure 2. Increased thomsbospondin-1 (TSP1) expression in mice after IH exposure.**

566 **A)** C57BL/6 mice were housed under normoxia or IH with or without infusion of Ang II for
567 28 days. Plasma concentration of TSP1 in mice detected by ELISA. **B)** *Thbs1* mRNA level in
568 left ventricle of mice exposed to IH with or without infusion of Ang II for 14 days quantified
569 by RT-PCR. **C)** C57BL/6 mice were housed under normoxia or IH with or without infusion of
570 Ang II for 28 days. The protein levels of TSP1, phosphorylated Smad2/3 (p-Smad2/3), and
571 total Smad2/3 (t-Smad2/3) in left ventricle of mice detected by western blot analysis. **D)**
572 Quantification of TSP1 and p-Smad2/3 in (C). **E)** Representative confocal microscopy images
573 of immunofluorescence staining for TSP1 and DAPI. Scale bar, 20 μm . **F)** Quantification of

TSP1 fluorescent intensity in (E). Data are mean \pm SEM, n=6 mice per group, *P<0.05, 2-way ANOVA with Bonferroni post-test. **G)** Quantification of number of cells negative for CD45, CD31, CD11b, and Ter119 and positive for Thy1 from left ventricle tissue digestion, that stained positive for intracellular TSP1 by flow cytometry. Data are mean \pm SEM, n=4, *P<0.05, unpaired 2-tail *t* test. **H)** Plasma concentration of TSP1 in healthy individuals and patients with obstructive sleep apnea (OSA) detected by ELISA. Data are mean \pm SEM, n=21, *P<0.05, unpaired 2-tail *t* test. Data used for quantitative analyses as well as the numerical data that are represented in graphs are available in Figure 2-source data.

Figure 3. IH induces cardiac fibroblast (CF) activation via TSP1.

A) Mouse primary CFs (mPCFs) were cultured under normoxia or IH for 24 hr. Representative confocal microscopy images of immunofluorescence stained for α -SMA, phalloidin and DAPI. Scale bar, 20 μ m. **B)** α -SMA fluorescence intensity quantification. **C)** Ratio of Ki67 positive cells to total mPCFs after IH exposure for 24h. Data are mean \pm SEM, n=5 independent experiments, *P<0.05, unpaired 2-tail *t* test. **D)** Quantification of gel contraction by mPCFs after IH exposure for 24hr. Data are mean \pm SEM, n=4 independent experiments, *P<0.05, unpaired 2-tail *t* test. **E)** *Thbs1* mRNA levels detected by RT-PCR. Data are mean \pm SEM, n=5 independent experiments, *P<0.05, unpaired 2-tail *t* test. **F)** Expression of TSP1 in mPCFs exposed to IH for the indicated time detected by western blot analysis. **G)** Quantification of TSP1 in (F). Data are mean \pm SEM, n=4 independent experiments, *P<0.05, 1-way ANOVA with Bonferroni post-test. **H-K)** mPCFs were infected with lentivirus to deliver *Thbs1* shRNA (LV-sh*Thbs1*) or control shRNA (LV-shCtrl) for 48 hr, then cultured under normoxia or IH for 24 hr. **H-I)** *Thbs1*, *Acta2*, *Col1a1*, *Postn* and *Tnfa* mRNA levels detected by RT-PCR. Data are mean \pm SEM, n=5 independent experiments, *P<0.05, 2-way ANOVA with Bonferroni post-test. **J)** Protein level of TSP1, collagen I (Col1), periostin and α -SMA detected by western blot analysis. **K)** Quantification of TSP1, Col1, periostin and α -SMA in J). Data are mean \pm SEM, n=4 independent experiments,

*P<0.05, 2-way ANOVA with Bonferroni post-test. Data used for quantitative analyses as well as the numerical data that are represented in graphs are available in Figure 3-source data.

Figure 4. IH induced STAT3 signaling activation in CFs.

A) mPCFs were cultured and exposed to IH for the indicated time. The protein levels of phosphorylated JAK1 at Tyr1034/1035 (p-JAK1^{Y1034/1035}), total JAK1 (t-JAK1), p-JAK2 at Tyr1008 (p-JAK2^{Y1008}), total JAK2 (t-JAK2), p-JAK3 at Tyr980/981 (p-JAK3^{Y980/981}), total JAK3 (t-JAK3), p-STAT3 at Tyr705 (p-STAT3^{Y705}) and Ser727 (p-STAT3^{S727}) and total STAT3 (t-STAT3) detected by western blot analysis. **B)** Quantification of indicated protein levels in (A). Data are mean \pm SEM, n=4 independent experiments, *P<0.05, 1-way ANOVA with Bonferroni post-test. **C-D)** mPCFs were cultured and exposed to IH for 1 hr with or without TG101209 (2 μ M). Indicated protein levels were analyzed (D). **E)** mPCFs were exposed to IH for 1 hr. Representative confocal microscopy images of immunofluorescence staining for STAT3 and DAPI. Scale bar, 20 μ m. **F)** Quantification of subcellular localization of STAT3 in (E). Data are mean \pm SEM, n=5 independent experiments, *P<0.05, unpaired 2-tail *t* test. **G)** The protein levels of p-STAT3^{Y705} and p-STAT3^{S727} in ventricles of mice with or without IH detected by western blot analysis. **H)** Quantification of p-STAT3^{Y705}, p-STAT3^{S727} and t-STAT3 in (E). Data are mean \pm SEM, n=6 mice per group, *P<0.05, unpaired 2-tail *t* test. **I)** Representative confocal microscopy images of immunofluorescence staining for STAT3, periostin, and DAPI in mice exposed IH with or without Ang II infusion for 4 weeks. The white arrows indicate periostin-positive cells with nuclear localization of STAT3. Scale bar, 10 μ m. Data used for quantitative analyses as well as the numerical data that are represented in graphs are available in Figure 4-source data 1.

Figure 5. Silencing and inactivating STAT3 downregulated TSP1 expression and attenuated IH-induced CF activation.

A-C) mPCFs were transduced with STAT3 siRNA (siSTAT3) or control siRNA (siCtrl) for 24

hr, then cultured under normoxia or IH for 24 hr. **A)** *Thbs1*, *Acta2*, *Colla1*, *Postn*, *Stat3* mRNA levels were quantified by RT-PCR. Data are mean \pm SEM, n=5 independent experiments, *P<0.05, 2-way ANOVA with Bonferroni post-test. **B)** The protein levels of TSP1, collagen I (Col1), periostin, STAT3 and α -SMA detected by western blot analysis. **C)** Quantification of TSP1, Col1, periostin, STAT3 and α -SMA protein level in (B). Data are mean \pm SEM, n=4 independent experiments, *P<0.05, 2-way ANOVA with Bonferroni post-test. **D-F)** mPCFs were cultured under normoxia and IH for 24 hr with or without S3I-201 (100 ng/mL). **D)** *Thbs1*, *Acta2*, *Colla1*, and *Postn*, mRNA levels detected by RT-PCR and quantified. Data are mean \pm SEM, n=5 independent experiments, *P<0.05, 2-way ANOVA with Bonferroni post-test. **E)** The protein levels of TSP1, Col1, periostin, and α -SMA detected by western blot analysis. **F)** Quantification of TSP1, Col1, periostin, and α -SMA protein level in (E). Data are mean \pm SEM, n=4 independent experiments, *P<0.05, 2-way ANOVA with Bonferroni post-test. Data used for quantitative analyses as well as the numerical data that are represented in graphs are available in Figure 5-source data.

Figure 6. STAT3 inhibitor ameliorated IH-induced cardiac fibrosis.

A) C57BL/6 mice exposed to IH with or without infusion of Ang II were treated with S3I-201 or vehicle. **B)** Ratio of heart weight to tibial length of mice. **C)** Quantification of ejection fraction (EF) after echocardiography of mice. **D)** Representative Masson staining of left ventricle of mice. Immunofluorescence staining of left ventricle for TSP1, periostin, Collagen I (Col1), α -SMA, VIME and DAPI. Scale bar, 100 μ m. **E)** Quantification of fibrotic area in Masson-stained slides (D), quantification of TSP1, periostin, and Col1 fluorescent intensity in (D), and quantification of co-localization of α -SMA and VIME in (D). **F)** Protein levels of TSP1, Col1, periostin, p-STAT3^{Y705}, t-STAT3 and α -SMA in left ventricle of mice detected by western blot analysis. **G)** Quantification of TSP1, Col1, periostin, p-STAT3^{Y705} and α -SMA in (F) Data are mean \pm SEM, n=6 mice per group, *p<0.05, 2-way ANOVA with Bonferroni post-test. **H)** Schematic diagram depicting the key findings of this study. IH induced cardiac

fibrosis via a STAT3/TSP1/Smad pathway. Data used for quantitative analyses as well as the numerical data that are represented in graphs are available in Figure 6-source data.

Figure 1-figure supplement 1

A) C57BL/6 mice exposed to intermittent hypoxia (IH) for 7 days. Mice were sacrificed 1 hr after pimonidazole injection. Representative confocal microscopy images of immunofluorescence staining for pimonidazole and DAPI. Scale bar, 100 μ m. **B)** C57BL/6 mice were housed under normoxia or IH with or without infusion of angiotensin II (Ang II) for 28 days. Quantification of cross-sectional area of cardiomyocytes in left ventricle. **C)** Ratio of TUNEL positive cells in left ventricle. Data are mean \pm SEM, n=6 mice per group, *p<0.05, 2-way ANOVA with Bonferroni post-test. Data used for quantitative analyses as well as the numerical data that are represented in graphs are available in Figure 1-figure supplement 1-source data.

Figure 5-figure supplement 1

A) mPCFs were cultured under normoxia and IH for 24hr. Chromatin immunoprecipitation (ChIP) quantitative PCR analysis of STAT3 binding on the Thbs1 genomic locus involved antibodies against STAT3, or rabbit IgG. The fold enrichment of the Thbs1 locus was determined by quantitative PCR and calculated as percentage of input. Data are mean \pm SEM (n=4 independent experiments). *P<0.05, unpaired 2-tail *t* test. Data used for quantitative analyses as well as the numerical data that are represented in graphs are available in Figure 5-figure supplement 1-source data.

Figure 6-figure supplement 1

A) C57BL/6 mice were treated with S3I-201 or vehicle for 14 days after exposure to IH and Ang II for 28 days. **B)** Ratio of heart weight to tibial length of mice. **C)** Quantification of ejection fraction (EF) after echocardiography of mice. **D)** Representative Masson and Sirius

red staining of left ventricle of mice. Scale bar, 100 μ m. **E)** Quantification of fibrotic area in Masson-stained slides (D). Data are mean \pm SEM, n=6 mice per group, *P<0.05, unpaired 2-tail *t* test. **F)** C57BL/6 mice infected with AAV9-periostin promoter-shStat3 (AAV9-Postn Prom-shStat3) or AAV9-periostin promoter-shScramble (AAV9-Postn Prom-shScramble) were exposed to IH with or without infusion of Ang II for 28 days. **G)** Quantification of number of cells negative for CD45, CD31, CD11b, and Ter119 and positive for Thy1 from left ventricle tissue digestion that stained positive for intracellular STAT3 by flow cytometry. Data are mean \pm SEM, n=6 mice per group, *P<0.05, unpaired 2-tail *t* test. **H)** Ratio of heart weight to tibial length of mice. **I)** Quantification of ejection fraction (EF) after echocardiography of mice. **J)** Representative Masson and Sirius red staining of left ventricle of mice. Scale bar, 100 μ m. **K)** Quantification of fibrotic area in Masson-stained slides (J). Data are mean \pm SEM, n=6 mice per group, *P<0.05, 2-way ANOVA with Bonferroni post-test. Data used for quantitative analyses as well as the numerical data that are represented in graphs are available in Figure 6-figure supplement 1-source data.

Supplementary File 1

RT-PCR primers

Figure 1

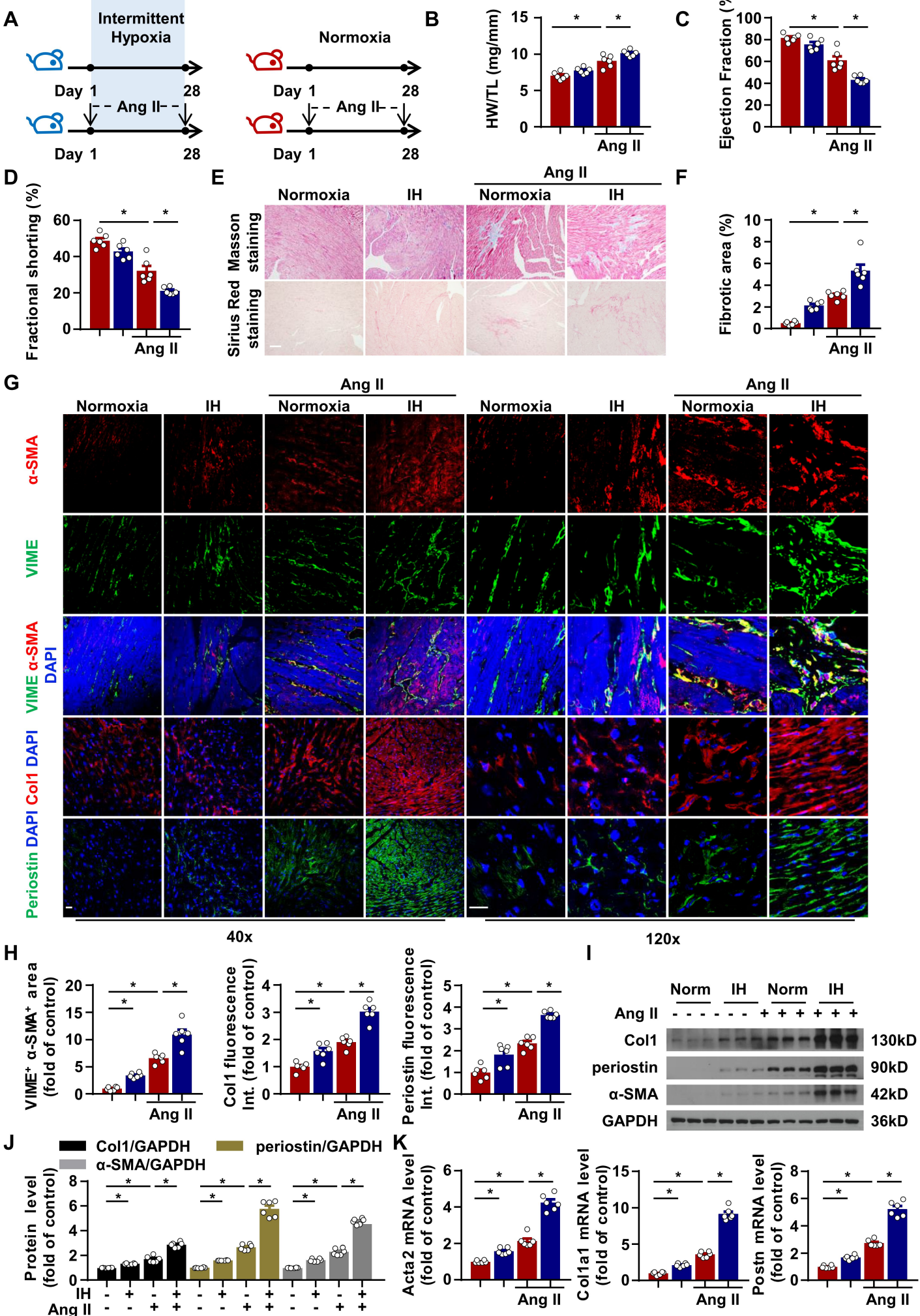
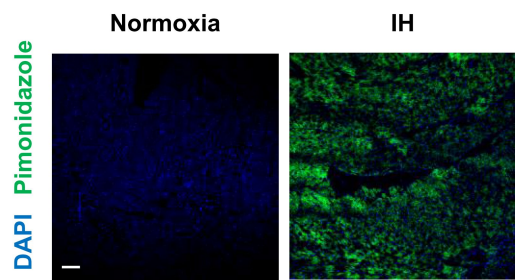
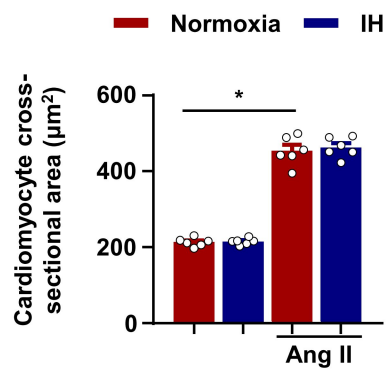


Figure 1-figure supplement 1

A



B



C

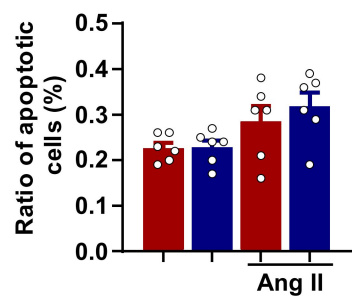


Figure 2 ■ Normoxia ■ IH

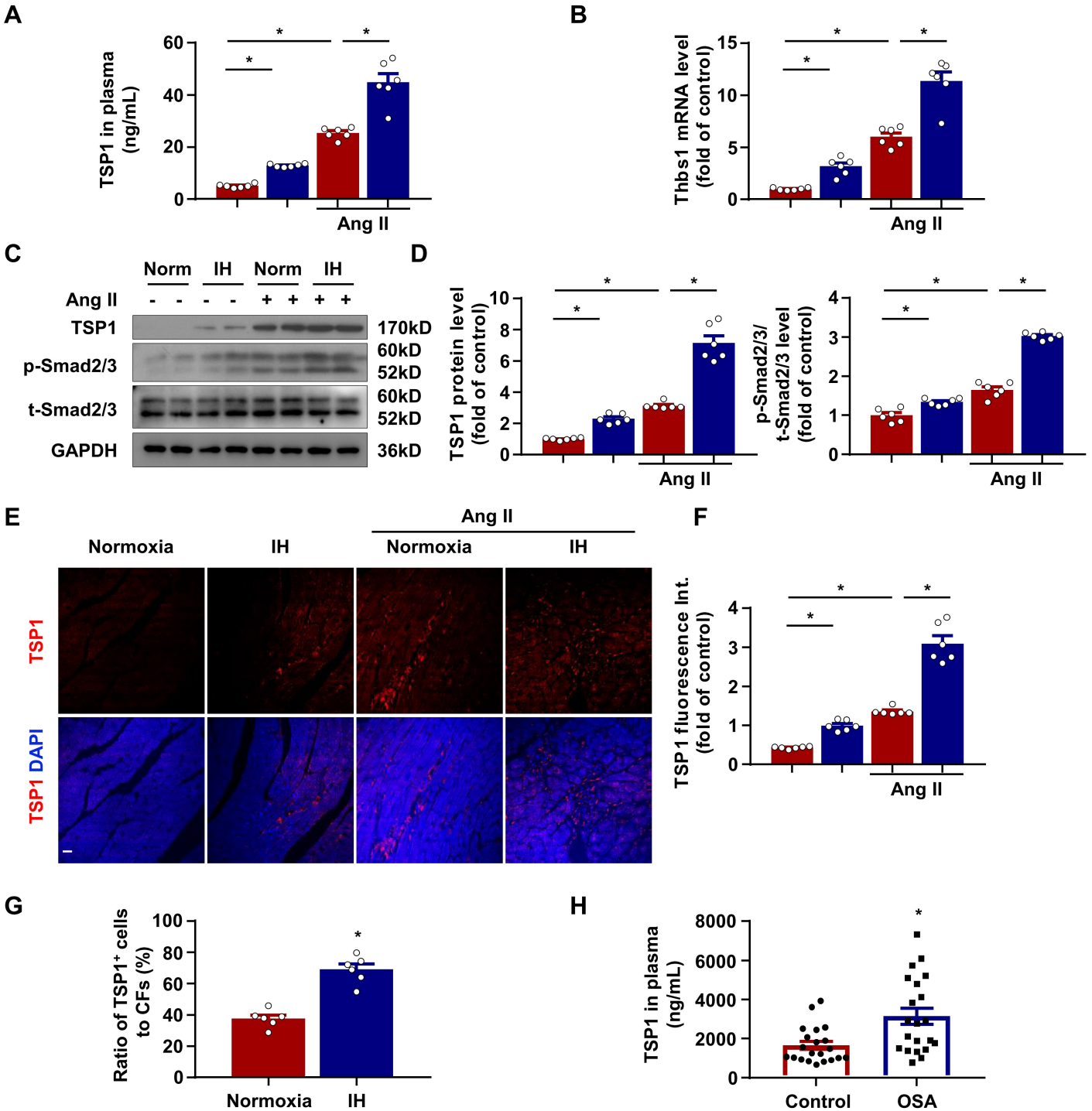


Figure 3

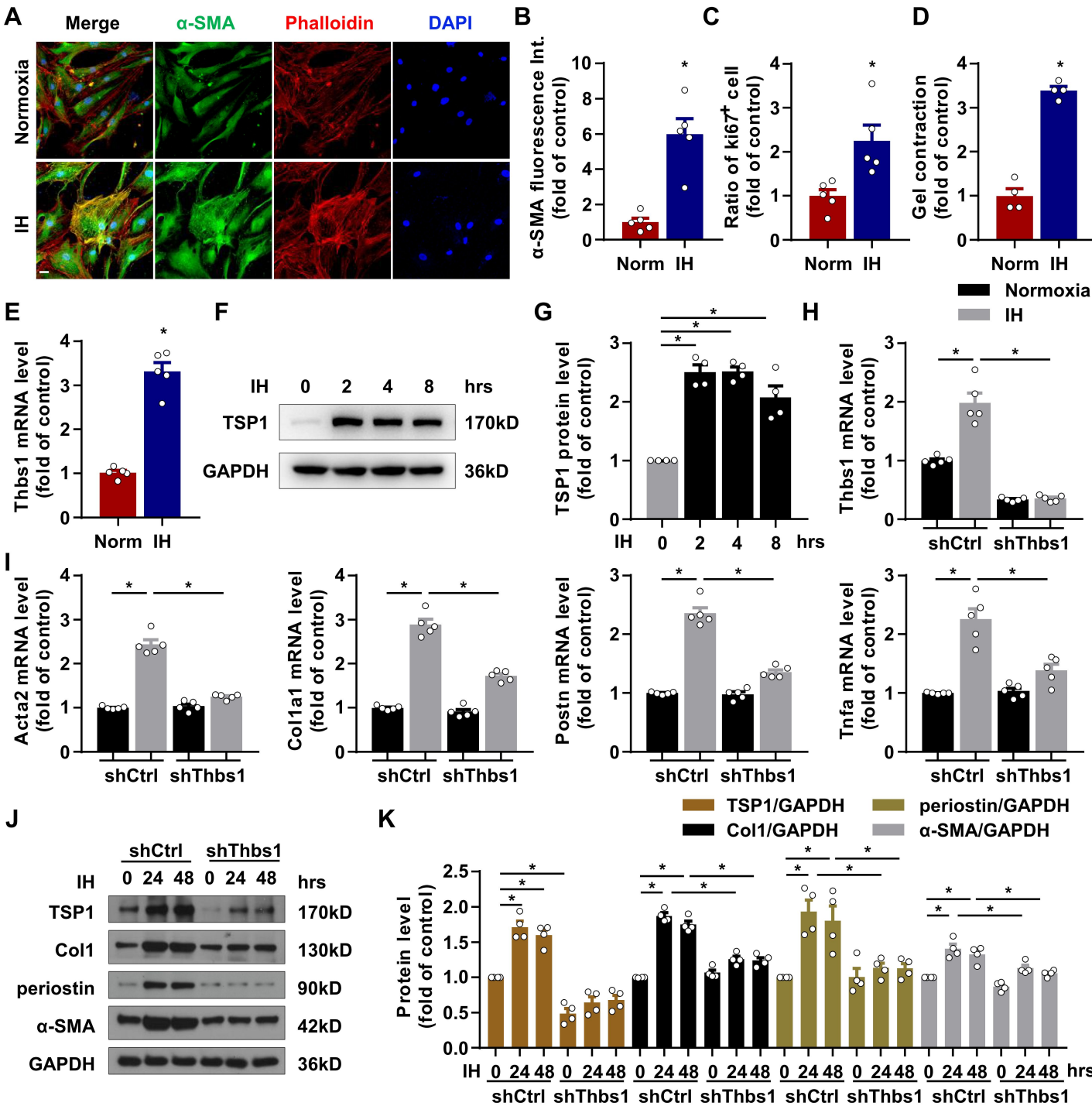


Figure 4

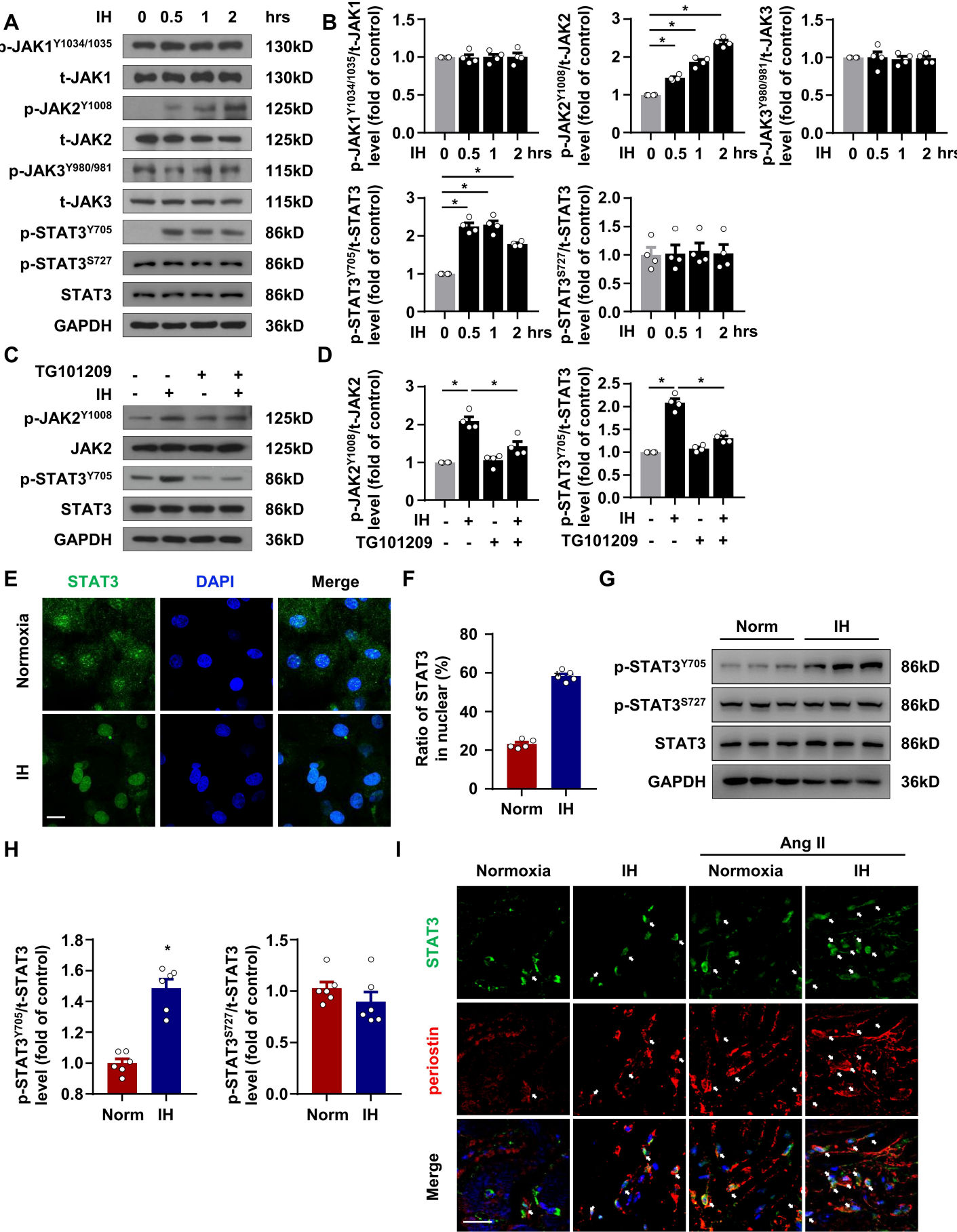


Figure 5

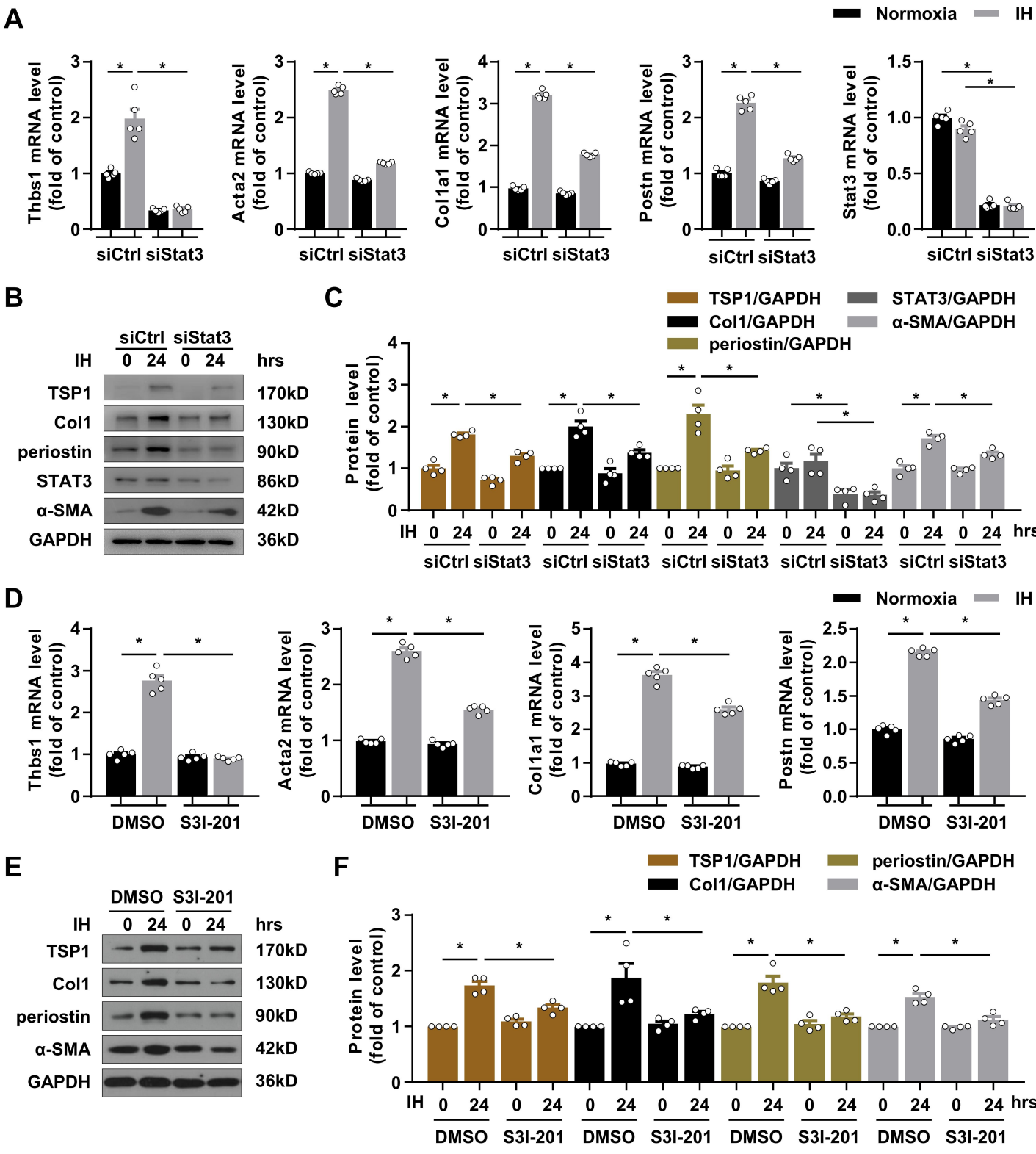


Figure 5-figure supplement 1

A

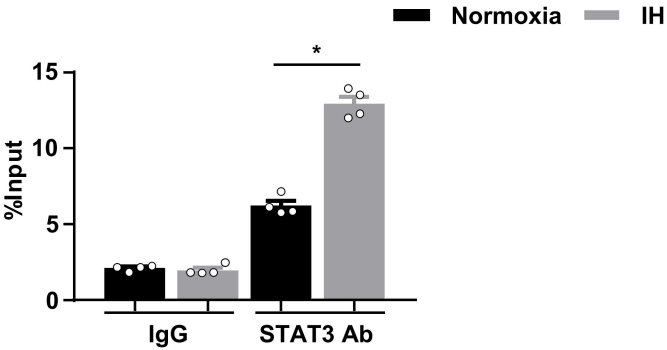


Figure 6

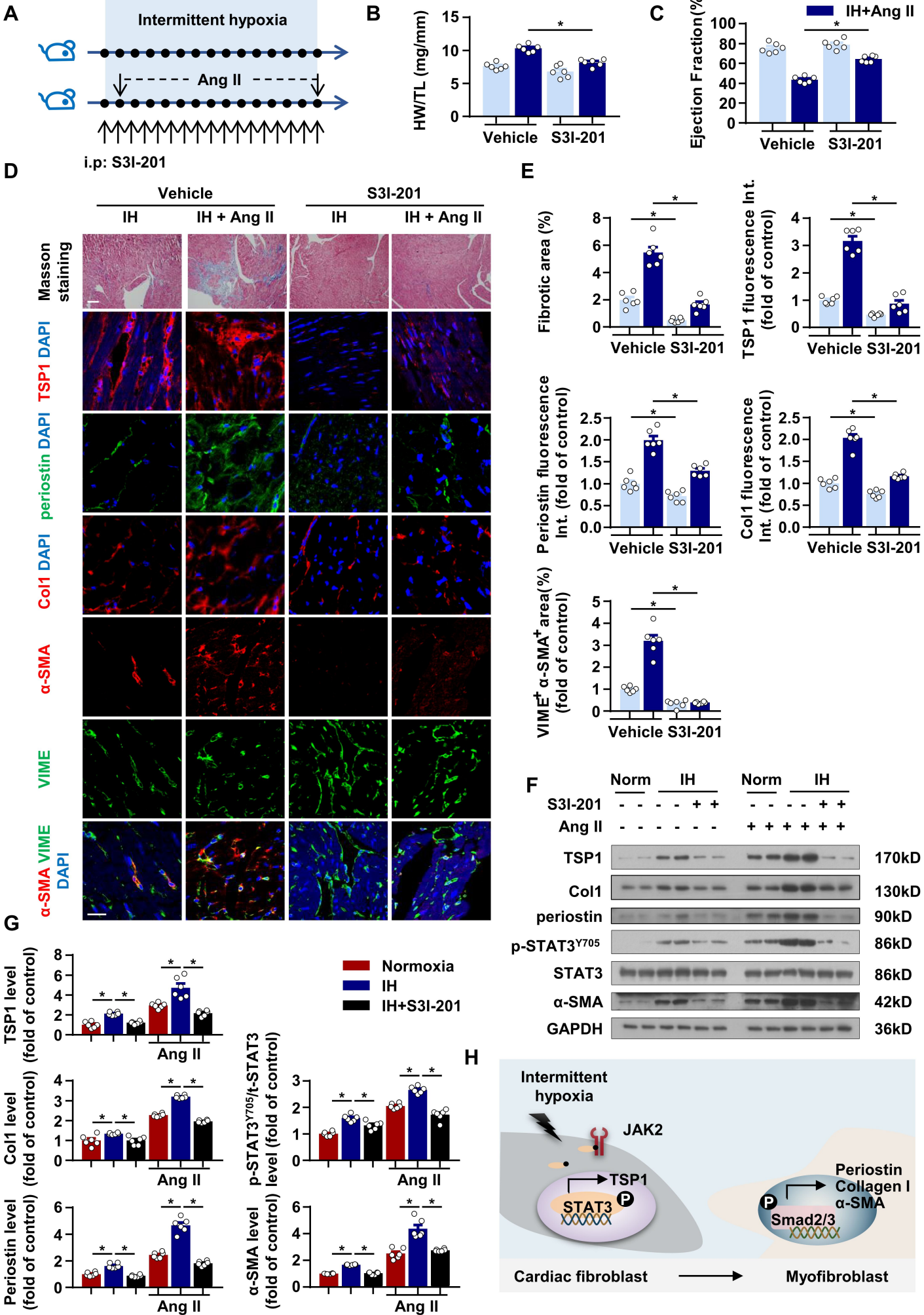


Figure 6-figure supplement 1

